Electronic Supplementary Material (ESI) for ChemComm.


**Supplementary Information**

# Modulation of destructive quantum interference by bridge groups in truxene-based single-molecule junctions

Lin Wang,*[a] Zhihao Zhao,[bc] Digambar B. Shinde,[d] Zhiping Lai,[d] and Dong Wang*[bc]

a School of Materials Science and Technology, China University of Geosciences, Beijing, 100083, China

b CAS Key Laboratory of Molecular Nanostructure and Nanotechnology and Beijing National Laboratory for Molecular Sciences, Institute of Chemistry, Chinese Academy of Sciences (CAS), Beijing, 100190, China

c University of Chinese Academy of Sciences Beijing, 100049, China

d Advanced Membranes and Porous Materials Center, Division of Physical Science and Engineering, King Abdullah University of Science and Technology (KAUST), Thuwal, Saudi Arabia.

## 1. Experimental details

### a. Synthesis of M3

The molecules **M1**, **M3** and **M4** were purchased from the Jilin Chinese Academy of Sciences - Yanshen Technology Co., Ltd. **M2** was synthesized according to the literature procedure.[1]

### b. Conductance Measurements

Molecule **M1** and **M3** were measured in the tetrahydrofuran (THF) and mesitylene (TMB) mixed solvent (volume ratio, $V_{THF}$: $V_{TMB}$ = 1:4). The **M2** and **M4** did not dissolve very well in THF so we changed the polar solvent to N, N-dimethylformamide (DMF) and kept the volume ratio. All the solvents were purchased from Sigma-Aldrich used without further purification. The STM gold tips were mechanically cut by gold wire (0.25 mm diameter, 99.95%). The substrates were 1 cm×1 cm silicon wafers with 100 nm gold evaporated on it (purchased from Beijing Top Vendor Science Technology Corporation). Both the tips and the substrates were washed by pure water and annealed just before use.

The conductance experiments were performed in a Pico4500 system (Molecular Imaging) STM using the PicoScan 5.3.3 software, with a 10 nA/V linear pre-amplifier (Agilent Technologies). The STM scanner was equilibrated with the room temperature for at least 30 min to reduce the impact of thermal drift. Conductance of the **M1**-**M4** were measured in a cell filled with about 0.1 mM molecular solution in ambient atmosphere. The cell was preliminarily dipped in 'piranha solution' (7:3 concentrated $H_2SO_4/H_2O_2$. *Caution: Mixing process is violently exothermic. Take care of it!*) and then washed by sonication in Milli-Q water (18.2 MΩ, TOC ≤ 4 ppb) for several times. Firstly, STM tip was lowered on the surface to a fixed set point current of 5 nA. Break junction experiments were then realized by controlling the tip scans from -4 nm to +1 nm relative to the original position.[2] After a short dwell time of 100 -200 ms, the tip was lifted with a velocity of 25 nm/s. Conductance versus displacement (G-s) data was recorded at 10 kHz sampling frequency during the tip moving up. Data selection and statistics analysis for histograms were conducted by MATLAB 7.0 and Originlab 8.5.

## 2. Data Acquisition and Analysis

### a. Details about Data Acquisition

All the traces were recorded consecutively and automatically. No selection has been done during the experiment. Both one-dimensional (1D) and two-dimensional (2D)

histograms constructed by all data were shown in Figure S1.

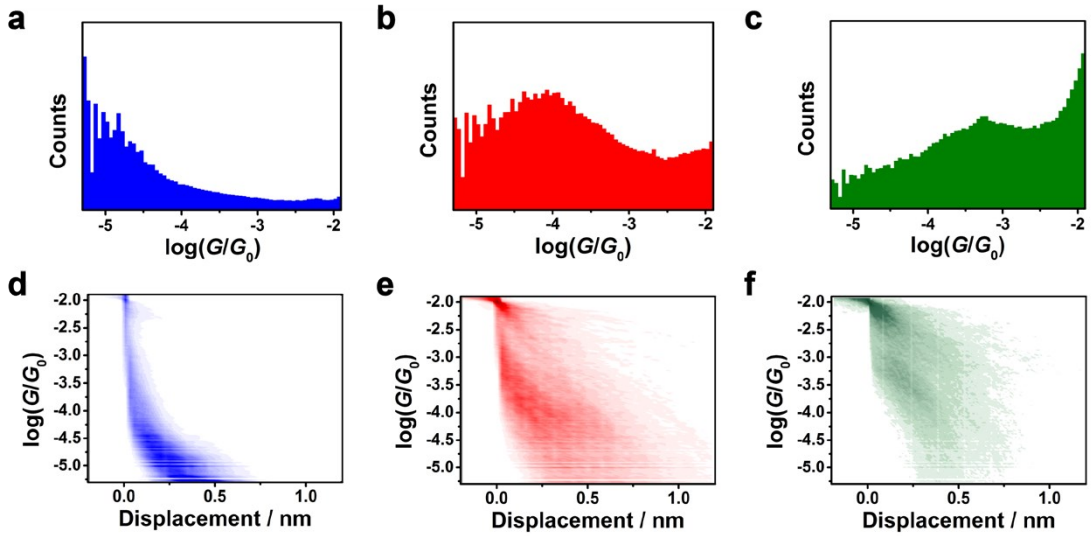


**Figure S1.** a-c) 1D and d-f) 2D (taking $10^{-2}$ $G_0$ as a relative zero point) conductance histograms of **M2-M4** based on the total conductance–distance curves without data selection.

## b. Selection of the Signal Curves

Although the conductance features can be recognized, 1D histograms exhibit high background and 2D histograms look noisier than those in Figure 2. Then the signal curves were selected manually for statistical analysis. Only curves with clear conductance features have been identified as 'signal curve' based on the criteria that they should contain at least one step longer than 0.05 nm at any region within our measurable conductance range (from $10^{-5.3}$ $G_0$ to $10^{-1.9}$ $G_0$). The conductance fluctuation was accepted with $\Delta\log(G/G_0) < 1.0$. The numbers of total curves and selected curves with conductance features are summarized below in Table S1.

**Table S1**. Selection of the conductance curves for **M2-M4**

| Molecules | Total Curves | Selected Curves | | Curves with Two Plateaus | |
|---|---|---|---|---|---|
| | | Number | Ratio | Number | Ratio |
| M2 | 6003 | 1084 | 18.1% | 58 | 1.0% |
| M3 | 2852 | 888 | 31.3% | 82 | 2.9% |
| M4 | 3137 | 691 | 22.0% | 29 | 0.9% |

## c. Conductance Curves with Two Plateaus

Most of the traces with the conductance feature have only one plateau. However, as displayed in Figure S2, we found very few numbers of curves (ratios are 1.0%, 2.9% and 0.9%) displaying two plateaus at the integer multiples of a fundamental current. This

phenomenon can be ascribed that two molecules have been bridged spontaneously between Au electrodes, and the molecular junction breaks in a stepwise fashion.[3] Curves with more than two plateaus were even scarcely observed (no more than five), indicating that it is difficult to accommodate more than two molecules in the junction. In the 1D conductance histogram, no shoulder peaks (dot line in Figure S2 d-f) whose most probably distributed conductance is corresponding to the double current can be identified. We believe that the majority of the current/conductance plateaus are due to the single molecules. The conductance peaks are symmetrically distributed, indicating that the broadening of the peaks is dominantly due to the geometric diversity of molecular junctions, rather than the formation of multi-molecule junctions.

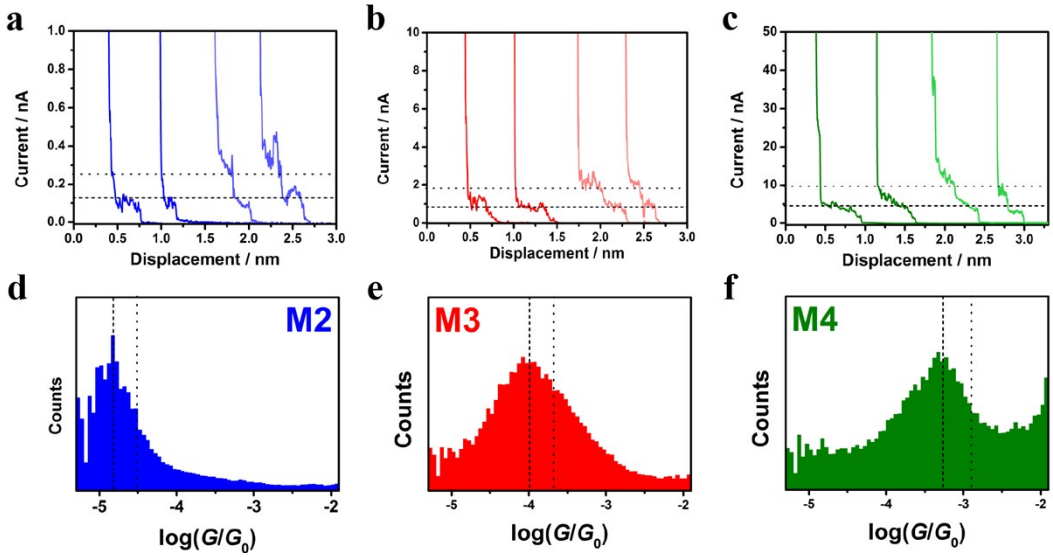


**Figure S2**. a-c) Typical conductance–distance curves (offset horizontally for clarity) exhibiting one and two plateaus. d-f) 1D conductance histograms for **M2**, **M3** and **M4**. Current and converted conductance values corresponding the fundamental plateaus are depicted by dash lines. Current and converted conductance values corresponding the double plateaus are depicted by dotted lines.

## 3. Theoretical Calculations

### a. Details for Simulation

All the optimized procedure and the transmission calculations were performed using Atomistix Tool Kit (ATK) and Virtual NanoLab software packages 13.8.0. Free molecule was firstly optimized to a force threshold of 0.01 eV $Å^{-1}$ for all atoms using DFT. To save the calculation time and system space, we decrease the length of the alkyl chains from six to two carbon atoms in **M2**. The exchange correlation functional was generalized gradient approximation (GGA). Subsequently, to construct a molecular device, we introduced the

molecule between a four-atom pyramid on the gold surfaces with a (6×6) super cell. As an initial guess, the amino group was chosen to locate on the adatom site with an Au-N bond length of 2.36 Å and a C-N-Au angle of 121.36 degrees.[4] The configuration of the **M4** molecular junction is showed in Figure S3. For structural optimization, we constrained all the Au electrode atoms in their bulk positions and optimized the molecular system until all maximum forces on each atom were smaller than 0.05 eV/ Å. In certain configurations (*cis* configurations for **M3,** see below), maximum force values were set to 0.06 eV/ Å or 0.07 eV/ Å for convergence. In the optimization process, two k-points in the irreducible part of the Brillouin zone for the x- and y-directions, and one k-point for the z-direction (the transport direction of the junction). Double-ζ (DZ) basis set for Au atoms and double-zeta plus polarization (DZP) basis set for the molecules were adopted in the calculation.[5] Then electron transport calculations of the device were performed by DFT combined with the non-equilibrium Green's function (NEGF) method. The mesh cutoff energy was set at 75 Hartree and k-points sampling (1×1×200) was adopted for x, y and z direction, respectively. GGA was used as exchange correlation functional.

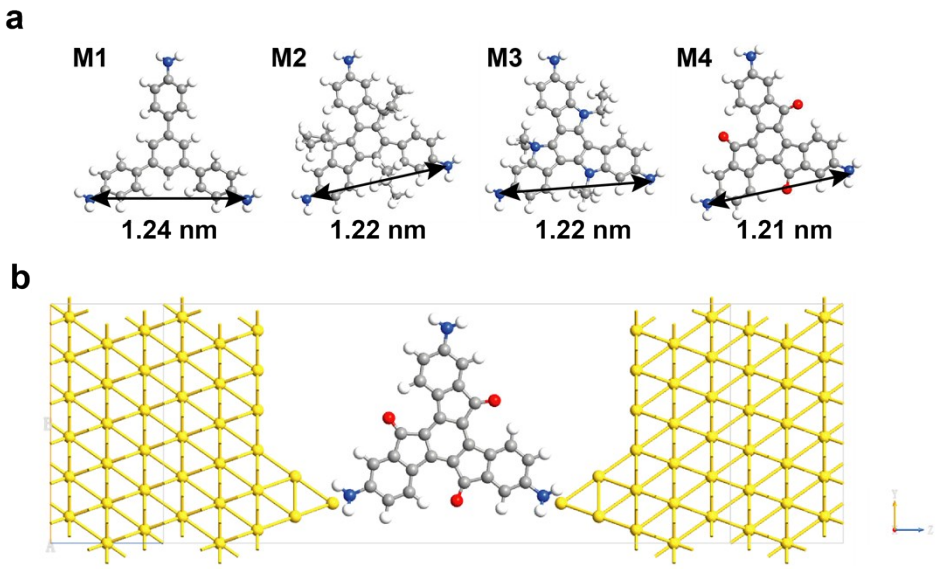


**Figure S3**. (a) Optimized molecule structure of **M1**-**M4**. The arrow shows the distance between N-N atoms. (b) Configuration of the Au/M4/Au molecular junction in our simulation.

### b. Molecular Projected Self-consistent Hamiltonian (MPSH) Analysis

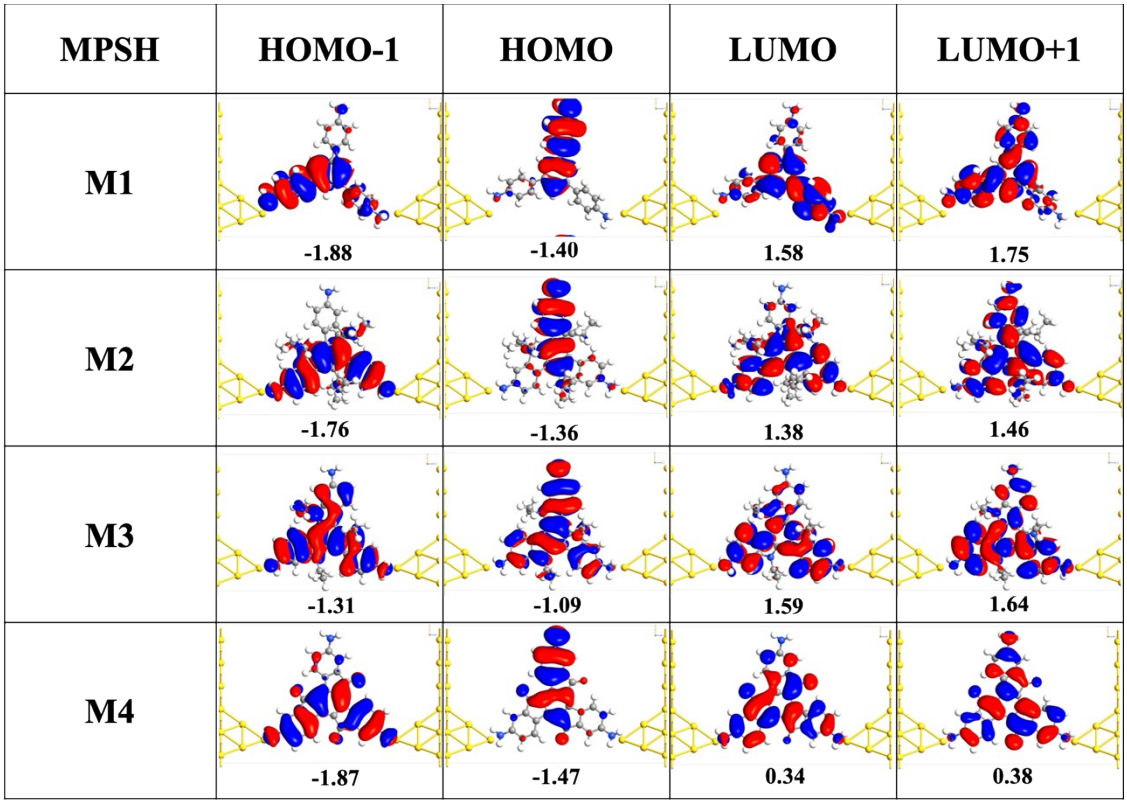


**Figure S4.** The spatial distribution of orbital levels modified by the electrodes, with an isovalue of 0.015.

**Table S2.** Results of **M1**-**M4** about frontier orbitals and single-molecule conductance.

| Molecule | Calculated HOMO (eV) | Calculated LUMO (eV) | $\Delta E_{DFT}$ (eV) | Experimental conductance ($G_0$) |
|---|---|---|---|---|
| M1 | -1.40 | 1.58 | 2.98 | $<10^{-5.3}$ |
| M2 | -1.36 | 1.38 | 2.74 | $10^{-4.8}$ |
| M3 | -1.09 | 1.59 | 2.68 | $10^{-4.0}$ |
| M4 | -1.47 | 0.34 | 1.81 | $10^{-3.3}$ |

### c. The Effect of Junction Structure on Transmission Function

We performed the transmission simulations by adjusting the atomic geometry of Au electrodes to explore the effect of molecular junction structure on electron transport properties. The molecular junctions are constructed based on the knowledge that the amino anchoring groups only bind to undercoordinated Au atop sites. Representative Au contact structures have been shown in Figure S5 and labeled as C1, C2 and C3.[6]

Transmission functions calculated based on various configurations are shown in Figure S6. We find that the energy position and the minimum of the anti-resonance valley fluctuate within a certain range for different molecular junction configurations. The energy fluctuation is no more than 0.5 eV and the transmission coefficient at the valley change

within one order of magnitude. We consider that the electron transport properties do not significantly depend on molecular configuration since the theoretical conductance trend of **M2**<**M3**<**M4** does not change for the junctions with similar configuration.

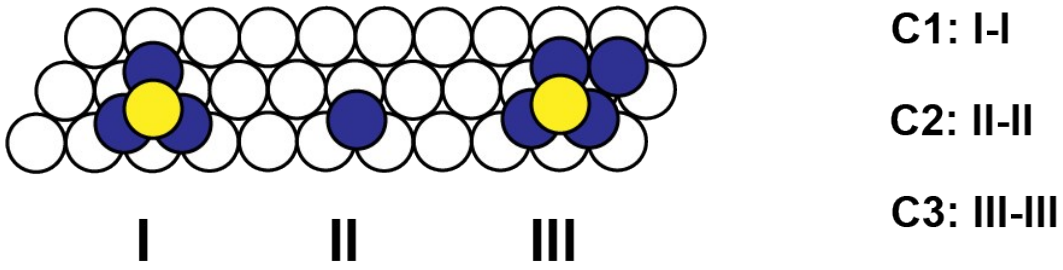


**Figure S5**. Contact motifs on gold electrode.

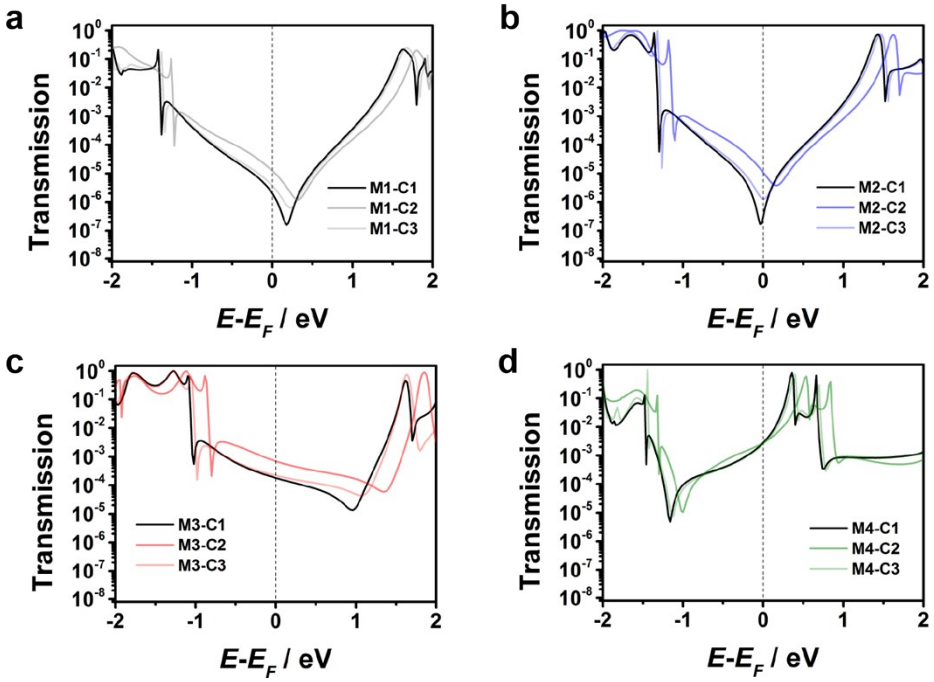


**Figure S6**. Transmission curves conducted by different configurations for **M1**-**M4**. The curves depicted by black solid line are the same with the ones in Figure 3 (in the manuscript).

### d. Discussion about the limitations of the calculations

Although more configurations of the molecular junction have been constructed for the transmission simulations, it is technically forbidden to survey all possibilities that occur in realistic conductance experiments. Asymmetric metal-molecule interface, the tilting molecule which causes stronger coupling between π system and the electrode, and other unexpected possibilities could also exist in realistic experiments. Additionally, it is difficult for the theoretical calculation to predict the most preferable configuration because the conductance calculation is performed based on the thermodynamically stable

configuration. However, the timescale of the molecular junction is within few milliseconds[7] for each curve so that dynamically stable configuration dominates the conductance experiments which may be difficult to capture by the steady-state calculation method.[5] Moreover, it has been reported that DFT cannot predict the position of the anti-resonance feature with fully accuracy because it is dependent on the basis group and the computational method.[5]

Although the molecular conductance cannot be exactly calculated, but information can be inferred from a qualitative view. Theoretical simulations in our work explain the conductance trend for **M2**<**M3**<**M4** in consistent with the experimental results. More quantitative analysis may be realized in future work by energy level-corrected DFT (DFT+∑) or other various levels of theory, such as Hartree-Fock, the many-body GW approximation and Hückel model.[8-10]

## References


1. I. Gadwal, G. Sheng, R. L. Thankamony, Y. Liu, H. Li and Z. Lai, *ACS Appl. Mater. Interfaces*, 2018, **10**, 12295-12299.
2. W. Haiss, R. J. Nichols, H. van Zalinge, S. J. Higgins, D. Bethell and D. J. Schiffrin, *Phys. Chem. Chem. Phys.*, 2004, **6**, 4330-4337.
3. B. Q. Xu and N. J. Tao, *Science*, 2003, **301**, 1221-1223.
4. N. Jing, L. Rui, S. Xin, Q. Zekan, H. Shimin, A. R. Rocha and S. Sanvito, *Nanotechnology*, 2007, **18**, 345203.
5. H. Li, M. H. Garner, Z. Shangguan, Y. Chen, Q. Zheng, T. Su, M. Neupane, T. Liu, M. L. Steigerwald, F. Ng, C. Nuckolls, S. Xiao, G. C. Solomon and L. Venkataraman, *J. Am. Chem. Soc.*, 2018, **140**, 15080-15088.
6. S. Y. Quek, L. Venkataraman, H. J. Choi, S. G. Louie, M. S. Hybertsen and J. B. Neaton, *Nano Lett.*, 2007, **7**, 3477-3482.
7. L. Venkataraman, J. E. Klare, C. Nuckolls, M. S. Hybertsen and M. L. Steigerwald, *Nature*, 2006, **442**, 904-907.
8. T. Markussen, J. Schiotz and K. S. Thygesen, *J. Chem. Phys.*, 2010, **132**, 224104.
9. C. Jin, M. Strange, T. Markussen, G. C. Solomon and K. S. Thygesen, *J. Chem. Phys.*, 2013, **139**, 184307.
10. T. Markussen, R. Stadler and K. S. Thygesen, *Nano Lett.*, 2010, **10**, 4260-4265.